

Northumbria Research Link

Citation: García-Burgos, Jimena, Miquelajauregui, Yosune, Vega, Elizabeth, Namdeo, Anil, Ruíz-Olivares, Alejandro, Mejía-Arangure, Juan Manuel, Resendiz-Martinez, Cinthia Gabriela, Hayes, Louise, Bramwell, Lindsay, Jaimes-Palomera, Monica, Entwistle, Jane, Núñez-Enríquez, Juan Carlos, Portas, Antonio and McNally, Richard (2022) Exploring the Spatial Distribution of Air Pollution and Its Association with Socioeconomic Status Indicators in Mexico City. *Sustainability*, 14 (22). p. 15320. ISSN 2071-1050

Published by: MDPI

URL: <https://doi.org/10.3390/su142215320> <<https://doi.org/10.3390/su142215320>>








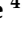
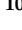

This version was downloaded from Northumbria Research Link: <https://nrl.northumbria.ac.uk/id/eprint/50686/>

Northumbria University has developed Northumbria Research Link (NRL) to enable users to access the University's research output. Copyright © and moral rights for items on NRL are retained by the individual author(s) and/or other copyright owners. Single copies of full items can be reproduced, displayed or performed, and given to third parties in any format or medium for personal research or study, educational, or not-for-profit purposes without prior permission or charge, provided the authors, title and full bibliographic details are given, as well as a hyperlink and/or URL to the original metadata page. The content must not be changed in any way. Full items must not be sold commercially in any format or medium without formal permission of the copyright holder. The full policy is available online: <http://nrl.northumbria.ac.uk/policies.html>

This document may differ from the final, published version of the research and has been made available online in accordance with publisher policies. To read and/or cite from the published version of the research, please visit the publisher's website (a subscription may be required.)

Article

Exploring the Spatial Distribution of Air Pollution and Its Association with Socioeconomic Status Indicators in Mexico City

Jimena García-Burgos ¹, Yosune Miquelajauregui ^{2,*}, Elizabeth Vega ³, Anil Namdeo ⁴, Alejandro Ruíz-Olivares ⁵, Juan Manuel Mejía-Arangure ^{6,7}, Cinthia Gabriela Resendiz-Martinez ⁸, Louise Hayes ⁹, Lindsay Bramwell ⁴, Monica Jaimes-Palomera ⁸, Jane Entwistle ⁴, Juan Carlos Núñez-Enríquez ¹⁰, Antonio Portas ¹¹ and Richard McNally ⁹

- ¹ Laboratorio de Ecología, Unidad de Biología de la Conservación, Parque Científico y Tecnológico de Yucatán, Universidad Nacional Autónoma de México (UNAM), Mérida 97302, Mexico
 - ² Laboratorio Nacional de Ciencias de la Sostenibilidad, Instituto de Ecología, Universidad Nacional Autónoma de México (UNAM), Mexico City 04510, Mexico
 - ³ Instituto de Ciencias de la Atmósfera y Cambio Climático, Universidad Nacional Autónoma de México (UNAM), Mexico City 04510, Mexico
 - ⁴ Department of Geography and Environmental Sciences, Northumbria University, Newcastle upon Tyne NE7 7XA, UK
 - ⁵ Department of Soil Sciences, Colegio de Postgraduados, Montecillo 56231, Mexico
 - ⁶ Facultad de Medicina, Universidad Nacional Autónoma de México (UNAM), Mexico City 04510, Mexico
 - ⁷ Genómica del Cáncer, Instituto Nacional de Medicina Genómica, Mexico City 14610, Mexico
 - ⁸ Secretaría de Medio Ambiente de la Ciudad de México, Mexico City 06068, Mexico
 - ⁹ Population Health Sciences Institute, Newcastle University, Newcastle upon Tyne NE1 7RU, UK
 - ¹⁰ Unidad de Investigación Médica en Epidemiología Clínica, UMAE Hospital de Pediatría Siglo XXI, Instituto Mexicano del Seguro Social (IMSS), Mexico City 06720, Mexico
 - ¹¹ Department of Mathematics, Physics and Electrical Engineering, Northumbria University, Newcastle upon Tyne NE7 7XA, UK
- * Correspondence: yosune@iecolologia.unam.mx



Citation: García-Burgos, J.; Miquelajauregui, Y.; Vega, E.; Namdeo, A.; Ruíz-Olivares, A.; Mejía-Arangure, J.M.; Resendiz-Martinez, C.G.; Hayes, L.; Bramwell, L.; Jaimes-Palomera, M.; et al. Exploring the Spatial Distribution of Air Pollution and Its Association with Socioeconomic Status Indicators in Mexico City. *Sustainability* **2022**, *14*, 15320. <https://doi.org/10.3390/su142215320>

Academic Editor: Giovanni Gualtieri

Received: 5 September 2022
Accepted: 11 November 2022
Published: 18 November 2022

Publisher's Note: MDPI stays neutral with regard to jurisdictional claims in published maps and institutional affiliations.



Copyright: © 2022 by the authors. Licensee MDPI, Basel, Switzerland. This article is an open access article distributed under the terms and conditions of the Creative Commons Attribution (CC BY) license (<https://creativecommons.org/licenses/by/4.0/>).

Abstract: Air pollution is one of the most challenging global sustainability problems in the world. Roughly 90% of global citizens live in areas that exceed the acceptable air pollution levels according to the World Health Organization air quality guidelines. However, socially disadvantaged groups are disproportionately located in areas exposed to higher levels of air pollution. Understanding the association between risk exposure to air pollutants and the underlying socio-economic factors determining risk is central for sustainable urban planning. The purpose of this study was to explore environmental inequalities in Mexico City, specifically the spatial association between air pollutants and socioeconomic status (SES) indicators. We propose that SES indicators will be expected to spatially cluster vulnerable individuals and groups into heavily polluted areas. To test this hypothesis, we used 2017–2019 data from governmental records to perform spatial interpolations to explore the spatial distribution of criteria pollutants. We carried out spatial autocorrelations of air pollutants and SES indicators using the bivariate Moran's I index. Our findings provide strong evidence of spatial heterogeneity in air pollution exposure in Mexico City. We found that socially deprived areas located in the southern periphery of Mexico City were exposed to higher ozone concentrations. On the contrary, wealthiest areas concentrated in the city center were exposed to greater concentrations of nitrogen dioxide and carbon monoxide. Our findings highlight the need for policy-driven approaches that take into consideration not only the geographic variability and meteorological dynamics associated with air pollution exposure, but also the management of socioeconomic risk factors aimed at reducing disparate exposure to air pollution and potential health impacts.

Keywords: environmental inequality; air pollution exposure; socioeconomic indicators; sustainable urban planning; Mexico City

1. Introduction

Air pollution is recognized as one of the greatest global sustainability problems of the 21st century. According to the World Health Organization (WHO), approximately 4.2 million deaths per year are attributable to air pollution [1]. Air pollution refers to the presence of small particles, chemical substances or gases in the atmosphere that are harmful to the health of human populations and other living beings [2]. Anthropogenic activities including traffic, waste burning, solid fuel combustion, industry and agrochemical activities emit high levels of criteria air pollutants (hereafter “air pollutants”) such as carbon monoxide (CO), particulate matter (PM, both PM_{2.5} and PM₁₀), sulfur dioxide (SO₂) and nitrogen dioxide (NO₂)—known as primary pollutants—into the atmosphere. Secondary air pollutants, such as ozone (O₃), are formed in the atmosphere by reactions among NO_x and volatile organic compounds in the presence of sunlight [3]. It is estimated that roughly 90% of global citizens live in areas that exceed the acceptable air pollution levels according to the World Health Organization (WHO) air quality guidelines [4,5]. However, numerous case studies have found that socially disadvantaged groups, such as persons and groups of lower socioeconomic status (SES), are disproportionately located in areas exposed to higher levels of air pollution, a phenomenon referred to as environmental injustice or environmental inequality [6–9].

Although the terms environmental injustice and environmental inequality are occasionally used interchangeably in the literature, they do have distinct meanings [10,11]. Environmental justice is a normative concept with political connotations that implies distributive (i.e., equitable distribution of resources and capacities to implement strategies), procedural (i.e., extent to which actors participate in decision-making processes) and precautionary (i.e., attitudes, values and judgments regarding environmental risks) justice levels [11–13]. Environmental inequality, on the other hand, is primarily a quantitative concept that involves measuring and comparing exposure risks among different individuals and groups [11,12]. In this paper, we focus on environmental inequality understood as disparities in air pollution exposure related to SES indicators.

In the context of urban air pollution, exposure risks derive from hazards that include pollutants emissions from transport, industry and domestic activities, wildfires and open burning among others [2]. However, in the literature regarding vulnerability, it is emphasized that risk (i.e., the probability of occurrence of an adverse event) emerges through the interactions between environmental conditions and socio-political factors [14,15]. This analytical framework recognizes that stakeholders actions and responses to hazards can also act as main determinants of risk [14,15]. In this perspective, risk exposure to air pollution in urban areas is not only a product of environmental hazards, but it is also shaped by socio-political processes including infrastructure and technological investment decisions (i.e., urban settlements, roads, highways, urban services, technology [16]) as well as mitigation and adaptation decision-making [13].

Environmental assessments are important analytical tools for effective exposure risk management generally conceived as centrally planned instruments aimed at supporting urban planning [17]. However, relevant environmental assessments for sustainable urban planning require providing evidence on the existence of systematic disparities in the distribution of risk exposure [8,10,17]. This need has motivated the development of integrated approaches capable of addressing disparities in environmental risk exposure across individuals and groups with differing SES [10,14]. For example, environmental inequality research in the context of air pollution has been mainly conducted in cities from North America, Europe, Asia and Oceania [17]. Results from these studies consistently report increasing exposure to air pollutants as SES decreased [18–22]. Only those from Europe [23] appear to find counterintuitive relationships between SES and air pollution as housing in historic city centers in Europe, that generally experience higher levels of atmospheric pollutants, has become unaffordable to individuals of lower SES [23]. However, studies carried out in cities from industrialized countries in Africa, Latin America and the Caribbean, which

often face uncontrolled urban sprawl, rampant population growth, increasing automobile emissions and consequently higher air pollution, are still scarce [17,19,24].

Despite these efforts, we still lack a full understanding of the association between risk exposure to air pollutants and the underlying socio-economic factors determining risk. This study aims to fill this knowledge gap by assessing whether in Mexico City—one of the most important economic hubs in Latin America—individuals and groups of lower SES are exposed to a higher burden of air pollution exposure. Thus, the purpose of this study is to explore environmental inequalities in Mexico City, specifically the spatial association between air pollutants and SES indicators. We posit that SES indicators will be expected to spatially cluster vulnerable populations into heavily polluted areas. To test this hypothesis, we conducted a set of spatial autocorrelations using 2017–2019 data from governmental records. Our methodological approach makes use of spatial analytic techniques that ensure independence among observations. We argue that the results of our study contribute to environmental inequality, a growing body of research aimed at analyzing the extent, causes and consequences of disproportional risk exposure among regions and populations. The analytical approach presented here can help to understand and make visible the socioeconomic inequalities in air pollution exposure to better derive and establish targeted sustainable urban planning interventions committed to environmental justice.

2. Methods

2.1. Study Setting

Mexico City is located at 19°35'34" N and 99°21'54" W (INEGI 2017), in the lower Basin of Mexico area, constituting an endorheic system surrounded by mountains. The Mexico City urbanized area occupies a surface of 2300 km² at 2240 m and has a current population of 9,209,944 inhabitants [25]. Urban expansion in Mexico City has been characterized by a horizontal occupation pattern that has progressively incorporated the rural peripheries which often display marked socioeconomic inequalities [26]. Mexico City has a cold dry season from November to February followed by a dry warm season from March to May and a wet season from June to October. Temperatures are moderate and vary little along the year [27,28]. Mexico City is the fifth largest urban area in the world and one of the most important economies in Latin America [29,30]. It is estimated that nearly 4 million mobile vehicles including public transport trucks, vans, cargo trucks and motorcycles and more than 88,000 industries which are located mostly in the northern areas of the city, operate daily (Figure 1) [29]. The transportation sector accounts for over 80% and 40% of NO_x and PM emissions, respectively [29], while industrial and domestic activities including the use of aerosol products and fuel burning are responsible for nearly 55% of volatile organic compounds (VOCs) emissions (Figure 1). Agriculture, construction and urban activities, including waste management and electrical energy generation, account for 36% to 46% of PM and 23% of VOCs emissions (Figure 1) [30]. Air pollution in Mexico City reached its peak during the 1980s and 1990s [31]. For more than 30 years, federal planning instruments and regulatory strategies have been designed and implemented with the aim at improving air quality in Mexico City [31]. Despite the efforts, air pollution has not been reduced enough to meet international and national standards, especially for PM and O₃ [29,31,32].

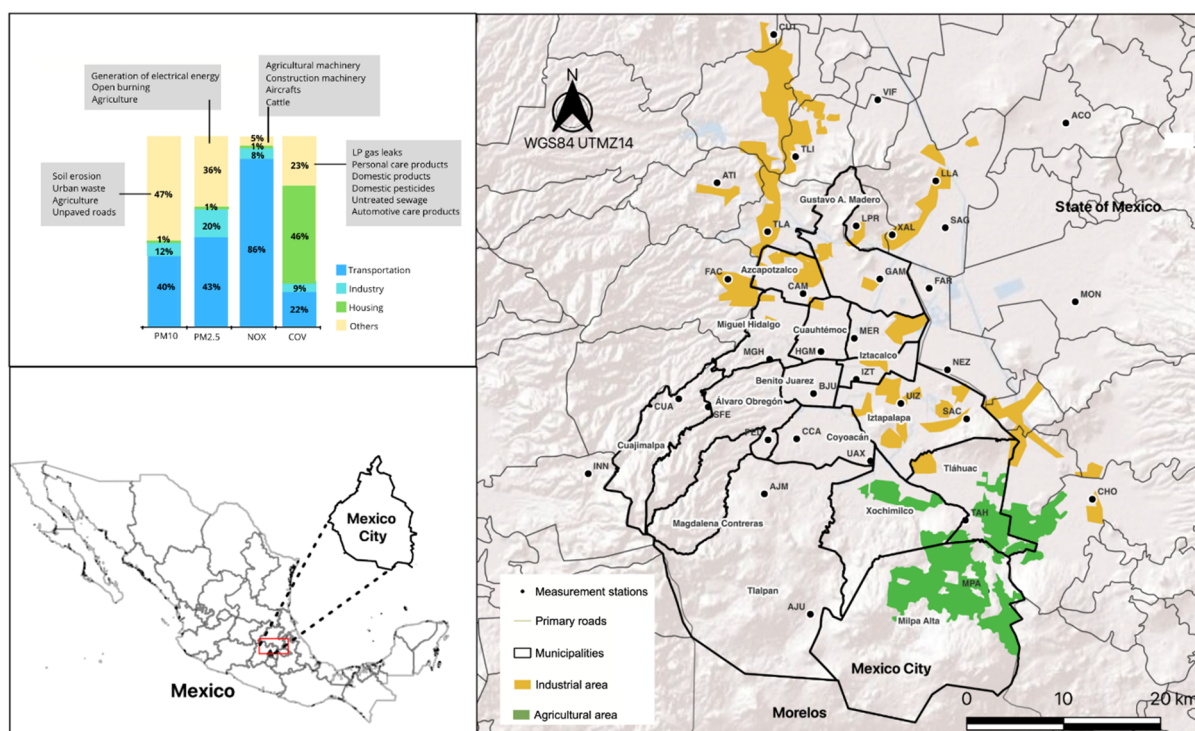


Figure 1. Mexico City showing the sixteen administrative units (bold lines) and the SIMAT monitoring stations (circles). Industrial (in yellow) and agricultural (in green) areas within Mexico City and the State of Mexico are also shown. The upper left panel indicates the distribution of air pollution sources by main activities (e.g., transportation, industry, domestic fuel burning).

2.2. Data

Air Pollution and Meteorological Data

A historical air quality dataset (2017–2019) was obtained from the Atmospheric Monitoring System (SIMAT, Figure 1), the main monitoring network in Mexico City. The monitoring network consists of 44 stations distributed within Mexico City (Figure 1). The air quality dataset included the monitoring station name and coordinates, the date of measurement, as well as hourly measurements of air pollutant concentrations, namely NO_2 ($\mu\text{g}/\text{m}^3$), CO (ppm), O_3 ($\mu\text{g}/\text{m}^3$), PM_{10} ($\mu\text{g}/\text{m}^3$), $\text{PM}_{2.5}$ ($\mu\text{g}/\text{m}^3$) and SO_2 ($\mu\text{g}/\text{m}^3$). For each pollutant, we selected a set of monitoring stations with at least 75% sufficiency of hourly measurement data [27]. In the case of SO_2 , less than 14% ($n = 6$) of monitoring stations met the sufficiency criterion, therefore this pollutant was excluded from further analysis. We calculated annual 2017–2019 average concentrations for O_3 , NO_2 and CO , and the 90th percentile of daily average concentrations for PM_{10} and $\text{PM}_{2.5}$. Summary statistics for selected pollutants are shown in Table 1.

Meteorological data (2017–2019) was derived from the Meteorology Network (RED-MET) formed by 26 monitoring stations distributed within Mexico City. The dataset included the monitoring station name, the date of measurement and hourly measurements of main surface variables, including temperature ($^\circ\text{C}$), relative humidity (%) and wind speed (m/s^2). We calculated annual averages for each surface variable and grouped them into three sets based on the season the measurement took place. We then intersected the average annual temperature, relative humidity, and wind speed by season with the NO_2 , CO , O_3 , PM_{10} and $\text{PM}_{2.5}$ calculated concentrations. Table A1 shows seasonal summary statistics of the analyzed meteorological variables.

Table 1. Selected monitoring stations from the Mexico City Atmospheric Monitoring System used to calculate 2017–2019 pollutants concentrations. Basic information for each station including ID, station name, coordinates, and elevation (m) is shown. The 90th percentile of daily average concentrations ($\mu\text{g}/\text{m}^3$) for PM_{10} and $\text{PM}_{2.5}$ and annual average concentrations (mean \pm sd) for CO (ppm), NO_2 ($\mu\text{g}/\text{m}^3$) and O_3 ($\mu\text{g}/\text{m}^3$). See Figure 1 for distribution of stations within Mexico City.

ID	Name	Lon	Lat	Elevation	PM_{10}	$\text{PM}_{2.5}$	CO	O_3	NO_2
ACO	Acolman	−98.91	19.63	2198	88	—	0.32 ± 0.22	26.65 ± 22	16.12 ± 9.2
AJM	Ajusco Medio	−99.20	19.27	2548	—	35	0.33 ± 0.20	39.33 ± 24.8	16.64 ± 9.1
AJU	Ajusco	−99.16	19.15	2942	—	37	—	35.41 ± 26.5	—
ATI	Atizapán	−99.25	19.57	2341	76	—	0.41 ± 0.35	27.81 ± 23.6	20.66 ± 11.3
BJU	Benito Juárez	−99.15	19.37	2249	69	41	0.49 ± 0.37	32.19 ± 29.7	24.16 ± 12.7
CAM	Camarones	−99.16	19.46	2233	87	46	0.53 ± 0.44	28.44 ± 29.1	31.49 ± 14.8
CCA	Centro de Ciencias de la Atmósfera	−99.17	19.32	2294	—	35	0.41 ± 0.30	32.75 ± 29.6	22.99 ± 11.1
CHO	Chalco	−98.88	19.26	2253	100	—	0.52 ± 0.42	29.33 ± 25.1	20.56 ± 9.5
CUA	Cuajimalpa	−99.29	19.36	2704	55	—	0.38 ± 0.27	30.64 ± 22	22.59 ± 12.2
CUT	Cuautitlán	−99.19	19.72	2263	94	—	—	28.02 ± 26.3	18.93 ± 11.3
FAC	FES Acatlán	−99.24	19.48	2299	70	—	0.52 ± 0.48	29.87 ± 26.3	24.54 ± 14.2
FAR	FES Aragón	−99.04	19.47	2230	—	—	—	34.6 ± 28.4	18.19 ± 11.2
GAM	Gustavo A. Madero	−99.09	19.48	2227	79	46	—	30.83 ± 29.6	23.58 ± 13.5
HGM	Hospital General de México	−99.15	19.41	2234	72	44	0.49 ± 0.39	30.83 ± 28.6	29.82 ± 14.4
INN	Investigaciones Nucleares	−99.38	19.29	3082	46	28	0.18 ± 0.11	38.69 ± 21.1	—
IZT	Iztacalco	−99.11	19.38	2238	68	—	0.59 ± 0.45	29.37 ± 28.7	29.37 ± 13.5
LLA	Los Laureles	−99.03	19.57	2230	—	—	0.48 ± 0.41	27.15 ± 25.8	23.75 ± 12.7
LPR	La Presa	−99.11	19.53	2302	—	—	0.65 ± 0.55	28.31 ± 25.7	—
MER	Merced	−99.11	19.42	2245	87	45	0.59 ± 0.45	26.96 ± 27.4	33.45 ± 14.8
MGH	Miguel Hidalgo	−99.20	19.40	2327	64	40	0.52 ± 0.40	28.24 ± 27	29.05 ± 14
MON	Montecillo	−98.90	19.46	2252	—	39	0.36 ± 0.37	31.71 ± 26.6	16.23 ± 10.1
MPA	Milpa Alta	−98.99	19.17	2594	67	38	0.23 ± 0.15	44.8 ± 23.5	6.36 ± 4.8
NEZ	Nezahualcóyotl	−99.02	19.39	2235	—	45	0.54 ± 0.48	28.39 ± 25.6	24.35 ± 12.7
PED	Pedregal	−99.20	19.32	2326	56	35	0.36 ± 0.26	35.9 ± 29.6	21.96 ± 11.6
SAC	Santiago Acahualtepec	−99.00	19.34	2293	—	—	0.42 ± 0.41	32.21 ± 25.5	21.28 ± 12.3
SAG	San Agustín	−99.03	19.53	2241	100	45	0.54 ± 0.43	26.94 ± 24.4	23.6 ± 11.9
SFE	Santa fe	−99.26	19.35	2599	62	37	0.31 ± 0.22	30.8 ± 25.5	21.8 ± 11.6
TAH	Tláhuac	−99.01	19.24	2297	88	—	0.41 ± 0.32	34.45 ± 27	17.6 ± 13.3
TLA	Tlalnepantla	−99.20	19.52	2311	86	44	0.54 ± 0.40	25.23 ± 23.9	31.04 ± 14.1
TLI	Tultitlán	−99.17	19.60	2313	99	—	0.47 ± 0.41	28.91 ± 26.6	25.17 ± 14.2
UAX	UAM Xochimilco	−99.10	19.30	2246	—	39	0.49 ± 0.33	32.51 ± 28.7	21.62 ± 11.7
UIZ	UAM Iztapalapa	−99.07	19.36	2221	72	43	0.51 ± 0.42	27.73 ± 26.4	26.71 ± 13.4
VIF	Villa de las Flores	−99.09	19.65	2242	105	—	0.39 ± 0.35	27.47 ± 23.3	18.47 ± 12.1
XAL	Xalostoc	−99.08	19.52	2160	134	54	0.7 ± 0.61	25.82 ± 24	30 ± 14.4

2.3. Socioeconomic Status Indicators

SES indicator data were obtained from the 2020 INEGI database at the census block (Áreas Geoestadísticas Básicas-AGEBs; by its name in Spanish) sub-municipality scale [25]. AGEBs represent the smallest administrative units in Mexico and are expected to be homogenous in terms of their SES characteristics [24]. We selected a set of SES indicators which best depicted the conditions of poverty and inequality to which a substantial proportion of the population lives in Mexico City. The SES indicators (Table 2; see Glossary in Appendix B) included: total population (POBTOT), male population (POPMAS), female population (POP_FEM), indigenous population (P_HOG_IND), afro-descendant population (POBAFRO), population with disabilities (PCON_DIS), population older than 60 years old (P_60YMAS), population of children younger than 5 years old (P_0A2 and P_3A5), population without access to health care (PSINDER), number of houses on dirt floors (VPH_PISOTI), number of houses without electricity (VPH_S_ELEC), number of houses without a drainage system (VPH_NODRAIN), number of houses without access to potable water (VPH_AGUAFV), number of houses lacking access to private motorized transport (VPH_NDACMM) and number of houses without access to communication technologies (VPH_SINTIC). In addition to these indicators, we included the Urban Marginalization Index (IMU2010) derived from the Consejo Nacional de Población [33]. The Urban Marginalization Index represents a compound measure built on different inequality dimensions such as access to education and health care, availability of first-order goods, and enjoyment of adequate housing rights. This index measures the severity of marginalization and can take negative or positive values, with higher positive values indicative of greater marginalization levels [33]. We performed a set of individual Pearson tests to evaluate significant correlations among SES indicators and to consequently avoid data redundancy. SES indicators with positive coefficients $r \leq 0.6$, indicating significant weak correlations ($\alpha = 0.05$), were kept for further analyses (Table A2).

Table 2. Summary statistics (mean, sd, minimum and maximum) for the SES indicators. * denotes selected indicators based on Pearson correlation coefficients $r \leq 0.6$ (see Table A2).

Indicator	Mean \pm SD	Minimum	Maximum
POBTOT	3847.02 \pm 2382.90	0	21,198
POBFEM	2012.79 \pm 1235.73	0	11,128
POBMAS	1834.22 \pm 1149.56	0	10,070
P_0A20	111.46 \pm 85.29	0	709
P_3A5	135.59 \pm 101.38	0	796
P_60YMAS	627.25 \pm 351.80	0	2703
PHOG_IND *	117.87 \pm 145.94	0	1430
PCON_DISC	206.84 \pm 136.71	0	810
PSINDER	1045.72 \pm 724.38	0	4713
VPH_PISOTI *	5.73 \pm 11.15	0	147
VPH_S_ELEC *	0.23 \pm 1.15	0	22
VPH_AGUAFV *	8.43 \pm 54.28	0	1236
VPH_NODREN *	1.14 \pm 4.29	0	79
VPH_NDACMM *	580.21 \pm 415.92	0	3025
VPH_SINTIC *	3.93 \pm 5.80	0	66
IMU2010 *	-0.63 \pm 0.54	-1.61	1.74

2.4. Spatial Distribution of Air Pollutants

We implemented spatial interpolations using the Kriging method to obtain the spatial distribution of the air pollutants analyzed. The Kriging method is a statistical technique widely used to determine the spatial variation of atmospheric pollutants while providing a measure of error [34]. Given the geographic complexity of Mexico City, this interpolation method is particularly recommended (SEDEMA, pers. obs). The Kriging method assumes that nearby points have less variance than those that are more distant in space [35]. This method obtains the influence of the values by solving Equations (A1) and (A2) [36] (see

Appendix B). The Kriging method calculates a semivariogram which depicts the autocorrelation of the observed sample points according to their similarity, meaning that the greater the similarity, the lower the variance [36,37]. Therefore, the semivariogram evaluates the fit of the statistical model in terms of its predictions [38]. The Kriging spatial technique approximates a theoretical semivariogram to an empirical one (which is obtained from the data) to quantify the autocorrelation of the observations. We used Equations (A1) and (A2) to fit individual statistical models to each pollutant and estimated the parameters for each corresponding theoretical semivariogram (Table A3).

2.5. Spatial Autocorrelations: Bivariate Moran's I Index

The bivariate Moran's I index is a useful metric that tests for spatial autocorrelation by quantifying the spatial dependence between two variables [39]. Therefore, spatial autocorrelation gives us an idea of the degree to which two features tend to be clustered together or evenly dispersed over a geographic space. We calculated the Moran's I statistic, given Equation (A3) (see Appendix B), which entails specifying a contiguity weight matrix [40]. We performed individual spatial autocorrelation analysis between each pollutant and each SES indicator. This procedure resulted in 40 tests. The bivariate Moran's I index is interpreted similarly to the univariate Moran Index. That is, given a set of entities and an associated attribute, it evaluates whether the pattern is clustered, sparse or random. The domain of the bivariate Moran's I index is $[-1, +1]$, where the autocorrelation is positive when $I > 0$ and the spatial pattern is clustered; it is negative when $I < 0$ and the spatial pattern is heterogeneous; and null when $I = 0$ or values very close to 0. However, the bivariate Moran's I index can hide local patterns of spatial clustering which can represent a serious flaw when dealing with a large spatial dataset [39]. As a result, the local version of Moran's I index, normally referred to Local Indicators of Spatial Association (LISA), was used [41]. The LISA values provide a measure of the level of significant spatial clustering relative to the values that are located around that observation. In other words, it uses the local Moran's I index to geographically locate spatial clusters. The LISA is constructed from two Cartesian axes, representing on the X axis the normalized values of variable 1, and on the Y axis, the values of the lag or spatial lagged of variable 2. The lagged or spatial lag is the mean value of the standardized variable in all its neighboring spatial units which is needed to analyze a variable based on its neighbors. We then used Moran scatterplots to visualize and identify the degree of spatial autocorrelations among air pollutants and SES indicators. The Moran scatterplot is a neighborhood view approach that shows the distribution of points in four quadrants centered on the global mean: (1) high values surrounded by high values (HH; hotspots- environmental inequalities), (2) low values surrounded by high values (LH; outliers), (3) low values surrounded by low values (LL; coldspots) and (4) high values surrounded by low values (HL; outliers) [41]. All data manipulations and spatial analysis were implemented in R software version 4.1.1 [42] and in a free Geographic Information System (GIS) software named GeoDaTM [43].

2.6. Seasonal and Meteorological Effects on Air Pollutants' Concentrations

To complement the spatial analysis presented in the previous sections, we evaluated seasonal and meteorological relative effects on O_3 , NO_2 , CO, PM_{10} and $PM_{2.5}$ concentrations (response variables). We fitted linear regression models to the data and performed associated ANOVAs to test for significant impacts of the year (factor with 3 levels 2017, 2018 and 2019), season (factor with 3 levels: dry cold, dry warm and wet), temperature (continuous), relative humidity (continuous) and wind speed (continuous) on the response variables. All analyses were carried out in R [44].

3. Results

3.1. Spatial Distribution of Air Pollution Exposure in Mexico City

The spatial interpolations showed that exposure to air pollutants displayed distinctive distribution patterns over Mexico City (Figure 2). Average 2017–2019 NO_2 and CO exposure

was greatest in the northern and center parts of Mexico City, with average concentration values ranging from 21 to 33 $\mu\text{g}/\text{m}^3$ and 0.52 to 0.68 ppm, respectively, and decreasing in the southern parts with average concentrations between 6.3 to 21 $\mu\text{g}/\text{m}^3$ and 0.19 to 0.41 ppm, respectively (Figure 2a,b). In the case of O_3 , exposure was more pronounced in the southern part of the city, with concentrations ranging from 34 to 44 $\mu\text{g}/\text{m}^3$, decreasing in the north with average concentration values from 26 to 32 $\mu\text{g}/\text{m}^3$ (Figure 3c). In the case of PM_{10} and $\text{PM}_{2.5}$, the highest concentrations were observed in the northern and eastern parts of the city, with values from 76 to 100 $\mu\text{g}/\text{m}^3$ and 40 to 50 $\mu\text{g}/\text{m}^3$, respectively, whereas the lowest concentrations were observed in the southern and western parts of the city, with values from 46 to 70 $\mu\text{g}/\text{m}^3$ and 28 to 38 $\mu\text{g}/\text{m}^3$ (Figure 2d,e). Figure 3 shows time-series plots displaying temporal patterns of the studied air pollutants from 2017 to 2019. For O_3 and $\text{PM}_{2.5}$, average concentrations often exceeded international standards with greater concentrations recorded during the dry warm season (Figure 3b,d). For the latter, discrete peaks exceeding national standards were observed during 2019. In the case of NO_2 and PM_{10} , temporal trends were dominated by annual seasonal patterns with the highest peaks observed during the dry cold season (Figure 4a,e). CO was the only pollutant which consistently remained below international and national air quality limits.

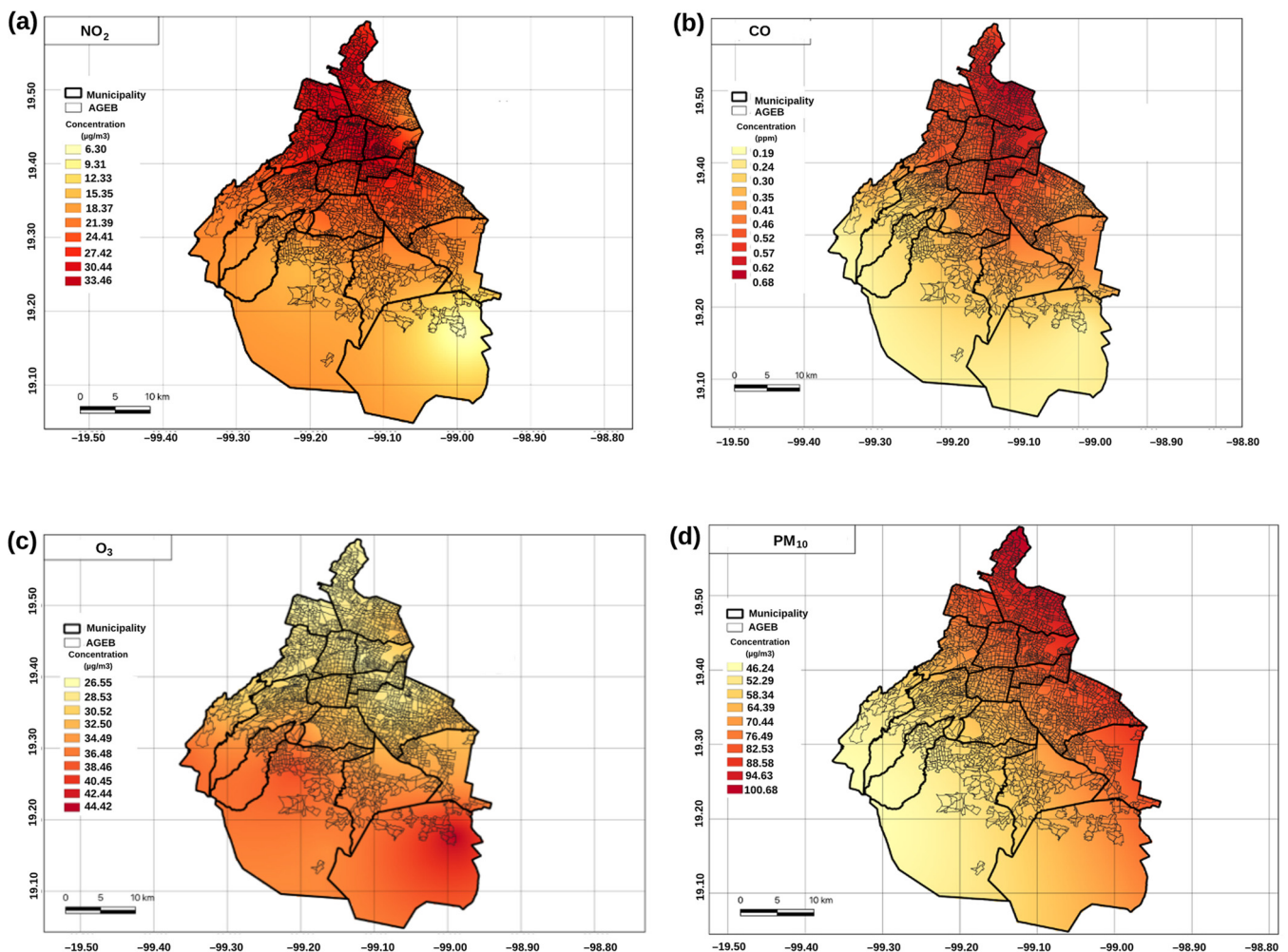


Figure 2. Cont.

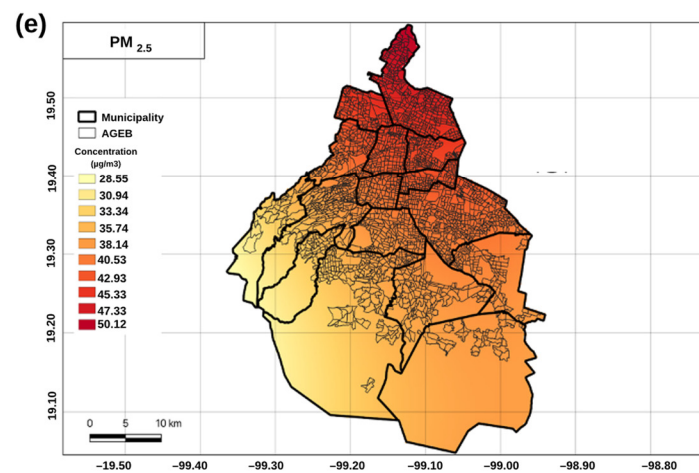


Figure 2. Spatial distribution of pollutants (a) NO_2 , (b) CO , (c) O_3 , (d) PM_{10} and (e) $\text{PM}_{2.5}$ in Mexico City resulting from the Kriging spatial interpolation analysis for 2017–2019. The thick lines correspond to the administrative municipalities and the thin lines to the AGEBs.

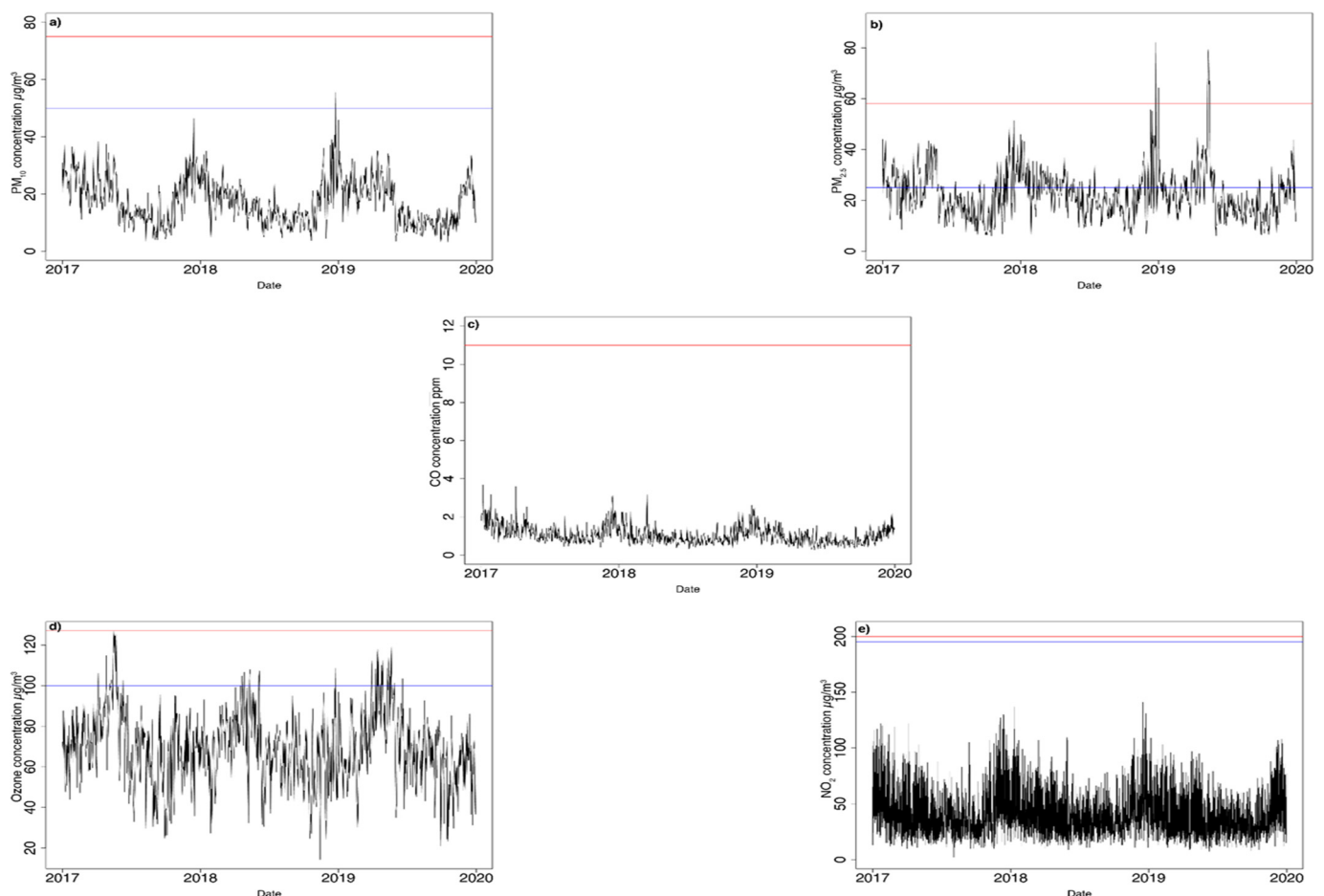


Figure 3. Time-series plots (2017–2019) displaying temporal variations in: (a) 24-h mean PM_{10} , (b) 24-h mean $\text{PM}_{2.5}$, (c) 8-h mean CO , (d) 8-h mean O_3 and (e) 1-h mean NO_2 . The red and blue lines correspond to limits according to the Official Mexican Standards (NOM) and the WHO air quality guidelines, respectively.

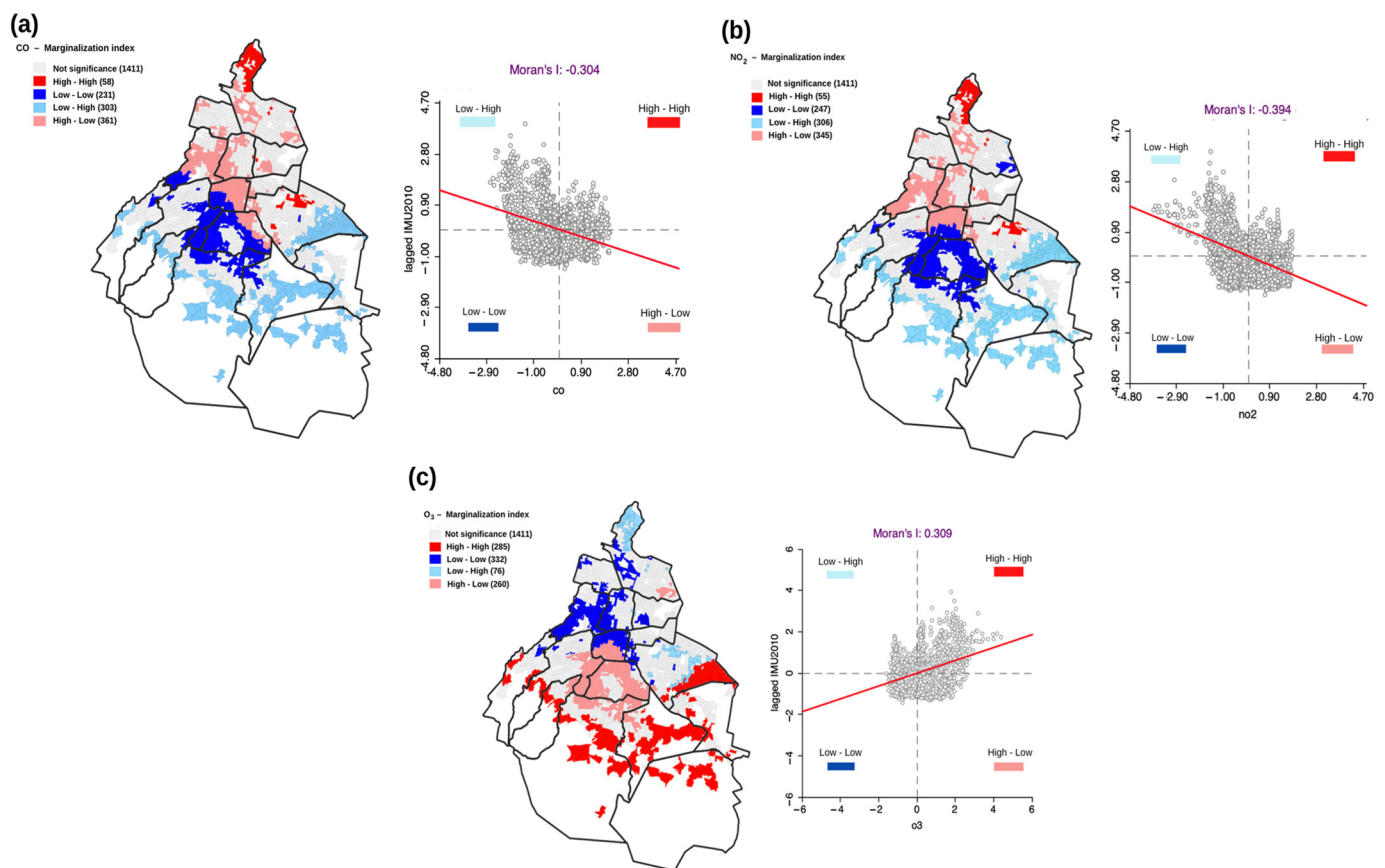


Figure 4. Local spatial autocorrelation of (a) NO_2 , (b) CO and (c) O_3 exposure by marginalization index levels (IMU2010) in Mexico City. Scatterplots consist of four quadrants: High–High (hotspots–environmental inequalities), Low–High (outliers), Low–Low (coldspots) and High–Low (outliers).

3.2. Seasonal and Meteorological Effects on Air Pollutants' Concentrations

The ANOVA results revealed significant seasonal and meteorological effects on the concentrations of pollutants. O_3 , PM_{10} , NO_2 and CO concentrations were significantly affected by season ($F = 36.7, 26.6, 4.9, 53.2, p < 0.05$, respectively). For $\text{PM}_{2.5}$, a significant interaction effect between year and season was also found ($F = 2.9, p = 0.02$). For these pollutants, highest mean concentrations ($38.4 \mu\text{g}/\text{m}^3, 53.3 \mu\text{g}/\text{m}^3, 26.4 \mu\text{g}/\text{m}^3, 0.47 \text{ ppm}$ and $27.1 \mu\text{g}/\text{m}^3$) were observed during the dry warm season, whereas lowest mean concentrations ($26.6 \mu\text{g}/\text{m}^3, 32.4 \mu\text{g}/\text{m}^3, 22.3 \mu\text{g}/\text{m}^3, 0.39 \text{ ppm}$ and $17.6 \mu\text{g}/\text{m}^3$) were observed during the wet season. Concerning the meteorological variables analyzed, we found a significant effect of temperature on O_3 , $\text{PM}_{2.5}$, NO_2 and CO concentrations ($F = 4.0, 5.9, 1.8, 25.0, p < 0.05$, respectively) and a significant effect of relative humidity on PM_{10} , $\text{PM}_{2.5}$, NO_2 and CO ($F = 5.6, 11.5, 4.3, 16.3, p < 0.05$, respectively). Wind speed had a significant effect on PM_{10} and $\text{PM}_{2.5}$ concentrations ($F = 12.0, 6.1, p < 0.05$, respectively).

3.3. Spatial Autocorrelation of Air Pollutants and SES Indicators

Most of the spatial autocorrelations between air pollutants and the SES indicators showed global Moran's I estimates of $-0.30 \leq I \leq 0.30$, which represent weak autocorrelations and were therefore considered as non-significant and excluded from further analyses. In other words, significant autocorrelations included bivariate. For those which resulted in significant values (Moran's I from -1 to -0.30 and 0.30 to 1), our analysis indicated positive spatial autocorrelations between O_3 and both IMU_2010 and VPH_PISOTI (Table 3).

Table 3. Bivariate Moran’s I index between air pollutants and socioeconomic status indicators. Numbers in bold represent significant associations.

SES Indicator	Pollutant				
	NO ₂	CO	O ₃	PM ₁₀	PM _{2.5}
P_HOG_IND	−0.25	−0.23	0.22	−0.02	−0.19
VPH_PISOTI	−0.39	−0.33	0.35	−0.13	−0.13
VPH_S_ELEC	−0.13	−0.11	0.12	−0.05	−0.08
VPH_AGUAFV	−0.22	−0.28	0.22	−0.18	−0.23
VPH_NODRAIN	−0.23	−0.21	0.25	−0.11	−0.15
VPH_SINTIC	0.020	0.008	−0.05	0.11	0.02
VPH_NDACMM	−0.14	−0.12	0.10	0.03	−0.04
IMU2010	−0.39	−0.30	0.30	0.01	−0.17

P_HOG_IND: indigenous population; VPH_PISOTI: number of houses on dirt floors; VPH_S_ELEC: number of hoses without electricity; VPH_AGUAFV: number of houses without access to potable water; VPH_NODRAIN: number of houses without a drainage system; VPH_SINTIC: number of houses without access to communication technologies; VPH_NDACMM: number of houses lacking access to private motorized transport; IMU2010: urban marginalization index.

On the other hand, we found negative spatial autocorrelations between both pollutants NO₂ and CO, and the SES indicators IMU2010 and VPH_PISOTI (Table 3). The pollutants PM₁₀ and PM_{2.5} were weakly associated with the SES indicators evaluated (Table 3). Figure 4 shows the local spatial autocorrelation between the air pollutants CO, NO₂ and O₃ and the SES indicator IMU2010, measured by the global Moran’s coefficient. Regarding CO, 15% of the AGEBs ($n = 361$) were distributed in the quadrant HL, indicating a cluster of spatial units exposed to high CO concentrations (cluster mean of 0.25 ppm), which are also characterized by low marginalization values (cluster mean of -1.2) according to the IMU2010 index (Figures 4a and 5). On the other hand, 3% of AGEBs ($n = 58$) were clustered in the HH quadrant (hotspots), indicating spatial units exposed to high CO concentrations (cluster mean of 0.54 ppm) characterized by high marginalization values (cluster mean = -0.04 ; Figures 4a and 5), while 22% of AGEBs ($n = 534$) were distributed in the LH and LL (coldspots) quadrants, indicating exposure to low CO concentrations.

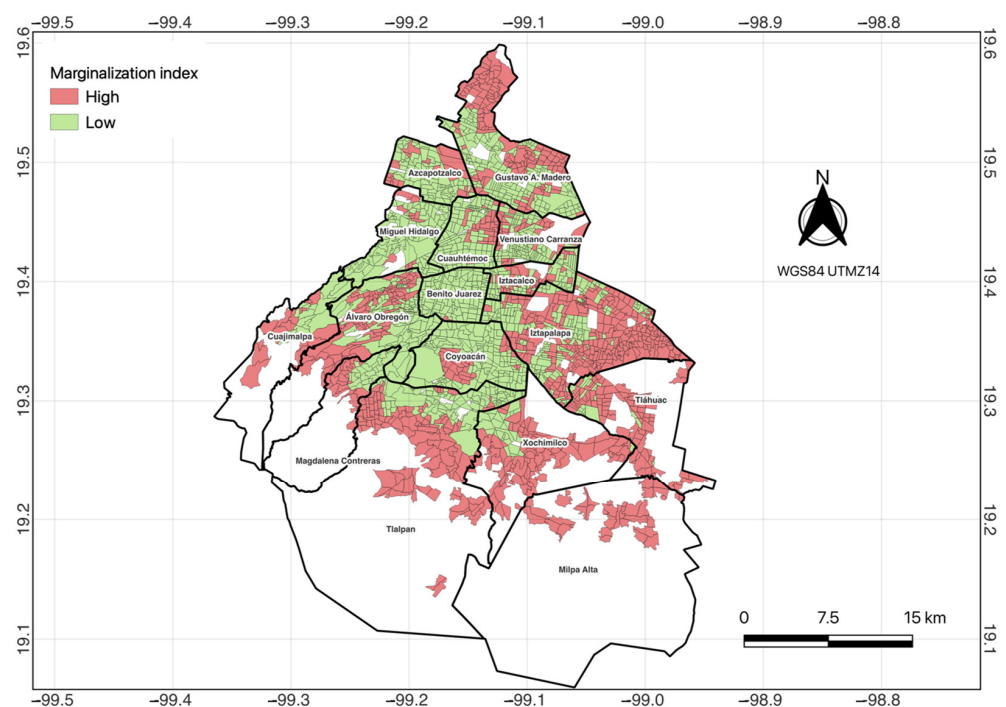


Figure 5. Distribution of marginalization index (IMU2010) in Mexico City.

Similar to the spatial patterns found for CO, the spatial analysis showed several HH and LL spots for the association between NO₂ and the SES indicator IMU2010, along with other areas in the HL and LH categories (Figure 4b). Overall, 14% ($n = 345$) and 2% of AGEBs ($n = 55$) were distributed in the HL and HH quadrants of the Moran's diagram, respectively, indicating spatial units exposed to high NO₂ concentrations (cluster mean of 29.0 and 28.2 $\mu\text{g}/\text{m}^3$, respectively). The former quadrant was characterized by low marginalization, whereas the latter to high marginalization values (cluster mean of -1.2 and -0.01 , respectively) according to the IMU2010 index (Figure 4b).

Regarding O₃, more than 26% of AGEBs were distributed in quadrants HH and HL ($n = 545$) of the Moran's diagram, indicating areas exposed to high concentrations of O₃ (cluster mean = 35 $\mu\text{g}/\text{m}^3$; Figure 4c). Of this percentage, nearly 52% of AGEBs ($n = 285$) were clustered in the quadrant HH, indicating areas exposed to high concentrations of O₃ (cluster mean = 37 $\mu\text{g}/\text{m}^3$) characterized by high marginalization values (cluster mean = 0.5) according to the IMU2010 (Figures 4c and 5). Similar spatial autocorrelation patterns were observed between CO, NO₂ and O₃ and the SES indicator VPH_PISOTI (Appendix A Figure A1).

4. Discussion

In this paper, we explored the socioeconomic inequalities in air pollution exposure in Mexico City through the use of spatial statistics tools and analysis. We performed Kriging interpolations to assess spatial distribution patterns of NO₂, CO, O₃, PM₁₀ and PM_{2.5} over Mexico City for the period 2017–2019. We then implemented spatial autocorrelations to evaluate the spatial association among air pollutants and a set of SES indicators. We also assessed seasonal and meteorological effects on the concentration of air pollutants, and identified specific time periods when risk exposure to air pollution increased. This study highlights the importance of incorporating spatial dynamics associated with air pollution combined with socioeconomic asymmetries when evaluating exposure risks.

4.1. Spatial Distribution of Air Pollutions Exposure in Mexico City

The spatial interpolations showed that air pollutants displayed distinctive distribution patterns over Mexico City (Figure 2), consistent with findings from other studies [17–23,31]. Ref. [44] explored differences in the spatial distribution of gaseous air pollutants in urban centers and explained the observed variations in terms of the physicochemical properties of pollutants, the rate of emission and reaction as well as meteorological factors such as wind direction. In their study, concentrations of inert pollutants such as CO decreased in downwind areas as they diluted with ambient air. For more reactive pollutants, such as NO₂, the production rate was identified as a critical parameter that was able to slow down the dilution process, thus concentrations decreased more gradually in downwind areas. In Mexico City, prevailing winds blow from the north to the south [33], transporting NO₂, CO and O₃ precursors which are emitted mostly by industrial and transportation activities in the northern and central parts of the city [27,28,30,31] (Figure 1). In the urban atmosphere, the distribution of ozone O₃ varies with both the intensity of solar radiation and the concentrations of precursor compounds such as NO_x and VOCs [44].

Ref. [45] studied changes in O₃ concentrations in both outdoor and indoor environments, concluding that seasonal changes in air movement, cloud cover, humidity along with emission rates of reactive VOCs and NO_x can alter ozone concentrations in the atmosphere. Additionally, empirical studies performed in urban-rural environments have demonstrated that ozone concentrations tend to be lower in urban areas since the freshly emitted NO, from road traffic, can deplete ozone locally [46]. The higher O₃ concentration in the southern periphery of Mexico City reported in this study aligns with those findings. On the other hand, the spatial distribution of particulate matter depends mostly on the size [44]. Transportation activities along with particulates from agriculture, industry and suspended dust emitted from eroded areas are likely to explain the higher concentrations of PM in the northern and eastern parts of the city (Figure 1) [28,30,31]. In 2001, the Air

Quality Program ProAire was launched by the Mexico City Government as a public policy instrument aimed at reducing the concentration of air pollutants by improving vehicle fuel combustion, regulating traffic hours and facilitating greater institutional coordination [30]. The current ProAire program contains new measures and actions across eight themes from reduction in consumption, technology shifts and environmental education to capacity building and citizen participation. Overall, air quality has improved in Mexico City since 2001, with important reductions in CO and SO₂ emissions [28]. The time-series plots (Figure 3) showing pollutants concentrations from 2017–2019 are consistent with those observations. In this line of thinking, it is worth noticing that CO was the sole pollutant that remained below international and national standards (Figure 3c).

Our findings provided strong evidence of spatial heterogeneity in air pollution exposure in Mexico City. The spatial patterns in air pollution exposure reported in this study can be partially explained by the observed seasonal variation in meteorological factors including temperature, relative humidity and wind speed. However, we acknowledge that the mechanisms and feedbacks behind the observed distribution of air pollution in Mexico City require further exploration. For instance, patterns of domestic and industrial energy use, efficiency in solid waste management actions, formal and informal land-use patterns and the location of green and blue urban infrastructure within the city, in addition to political factors including weak air pollution governance and agency, are potential factors explaining the observed distribution patterns in air pollution exposure in Mexico City [47,48]. Exposure to air pollutants is known to have detrimental long- and short-term effects on human health indicated by increases in hospital admissions for cardiovascular and respiratory diseases, asthma and reduced lung function among others [2,32]. Ref. [2] demonstrated that recurrent air pollution exposure, even to low concentration levels, can be extremely harmful for human health. In Mexico City, [24,32] a positive association between adverse health events and increased exposure to PM₁₀ and O₃ was revealed. Although outside the scope of this study, our results build upon the idea that recurrent exposure to air pollutants above recommended international and national limits, which mostly occur during the dry warm season, could exacerbate risk exposure, thus increasing the negative health outcomes reported for Mexico City (Figure 3).

4.2. Spatial Autocorrelations of Air Pollutants and SES Indicators

Our findings suggest the presence of socioeconomic disparities in air pollution exposure in Mexico City. Particularly, the southern periphery of Mexico City has emerged as an area of concern since 12% of AGEBs characterized by precarious socioeconomic conditions (Figure 4c) were also exposed to high ozone concentrations. These hotspots were mostly distributed in the administrative municipalities of Tlalpan, Milpa Alta, Xochimilco, Tláhuac, Cuajimalpa, Álvaro Obregón, Magdalena Contreras and Iztapalapa, where much of the conservation land (CL) is located. The CL is a space of high ecological value which covers nearly 50% of the total area of Mexico City [49]. During the past decades, the CL has undergone extensive urban expansion heavily marked by high population growth and increasing environmental deterioration [48,49]. From 1990 to 2020, the population in the CL almost doubled, with the highest growth rates taking place in the municipalities of Tlalpan and Tláhuac [48]. The CL population represents a sector at high risk of marginalization (Figure 5), characterized by greater job insecurity, deficits in water infrastructure (e.g., indoor plumbing and water supply), high levels of economic informality, lower education levels and shortages of household goods [50,51]. In these fast-growing areas, the lack of services, capacities and resources diminishes the likelihood of people to build robust strategies to mitigate air pollution [52]. In this perspective, mobilizing individuals for collective political actions represents an opportunity for developing locally-led solutions that promote environmental equity and justice [52,53].

The results of the LISA tests revealed a strong spatial association between CO and NO₂ exposure and the marginalization index in 2% to 3% of the AGEBs located in the northern portion of the municipality of Gustavo A. Madero (Figure 4a,b). Yet, 15% of AGEBs located

in the city's center (e.g., municipalities of Miguel Hidalgo, Cuauhtémoc and Benito Juárez) were also exposed to high concentrations of NO₂ and CO, highlighting a reverse trend than the rest of the city. This matches with some environmental studies found in Europe [22]. According to [22], European urban centers commonly developed in such a way that the wealthiest population sectors tended to occupy the city's central areas, where vehicular traffic and consequently NO₂ and CO emissions were more pronounced. In Mexico City, the financial and economic activities are primarily located in the city's center, the wealthiest core that sustains a significant proportion of all governmental and private services [25,52]. It is estimated that 70% of Mexico City's working age population commute daily to work to the city's central areas [53], increasing traffic load and associated pollutant emissions. Since most of the traveling takes place during busy hours, commuters are very likely to be exposed to high transport-related NO₂ and CO emissions [27,52].

Several studies have highlighted the uneven nature of risk exposure for different environmental stressors including air pollution [12,24,30,50]. Such is the case of those carried out in the United States, Canada and Australia which demonstrated that low-socioeconomic status populations were exposed to higher concentrations of O₃, CO and NO₂ [54,55]. Yet, opposite results have also been reported [17–24]. The nature of these discrepancies has been extensively discussed by [10] who identified two major sources of uncertainty when performing environmental justice studies. The first source of uncertainty relates to the spatial and temporal scale of the analysis, that is, the spatial analytical unit, while the second source corresponds to the choice of an appropriate methodological framework capable of dealing with spatial dependences. Thus, comparing and generalizing results can often be challenging. While the drivers conducive to varying spatial distributions in air pollution exposure might differ across regional and local scales, managing the socioeconomic risk factors is instrumental in reducing unequal air pollution exposure and informing sustainable urban planning interventions. In this line of thinking, we argue that urban planning interventions in Mexico City should be able to tackle the trade-offs between socioeconomic, environmental and health impacts of air pollution, while fostering equality and well-being primarily in informal settings.

4.3. Limitations and Future Research

In this study, we used observed (2017–2019) air pollutants concentrations together with spatial statistics tools and analysis to derive spatial distribution patterns of NO₂, CO, O₃, PM₁₀ and PM_{2.5}. This paper provides spatially explicit information on differentiated risk exposure to air pollution in Mexico City. We acknowledge that the resulting spatial patterns could have been improved by including long-term historical air pollution data. However, ensuring data sufficiency across monitoring stations for extended time periods was challenging in our case. An important limitation of our study concerns the spatial scale of the socioeconomic data we used to perform the spatial autocorrelations. Although the scale of AGEB was appropriate for this study given its fine resolution and homogeneity, there are few studies which monitor individual-scale exposure to air pollution on a daily basis [56].

The results presented here can be incorporated in further studies. For instance, diseases associated with air pollution represent a serious public health issue with important economic implications due to absences from productive work. Exploring differentiated health and economic impacts of air pollution in urban systems can help to design risk mitigation strategies specifically tailored to the needs and conditions of vulnerable individuals and groups. The role of innovation (social and technological) in reducing pollutants emissions is instrumental in reaching sustainability. However, innovation implementation faces significant challenges given the lack of procedures that facilitate the systematic integration of multiple stakeholders preferences and interests [57]. The latter emphasizes the increasing need to develop capacity building programs for effective participation in the process of air pollution control.

Climate change is expected to increase the frequency and severity of extreme weather events such as heat waves, wildfires and droughts worldwide [2]. Consequently, international and national efforts to meet the Sustainable Development Goals (SDGs), including those related to air pollution and human well-being, could be dampened. Analyzing the combined effects of climate change and air pollution is therefore critical to achieve sustainable urban systems. Future environmental assessment studies for sustainable urban planning need to also investigate the political and economic factors associated with air pollution exposure and the associated cascading risks [16]. These studies should focus not only on analyzing how risk exposure is negotiated but also how resources and mitigation costs are distributed within socially complex and highly uncertain contexts [13]. These types of studies can shed light on why pollutant sources have been historically placed in underprivileged neighborhoods characterized by acute shortages of services and poor access to local resources such as health care.

5. Conclusions

Environmental assessments for sustainable urban planning require providing evidence on the existence of systematic disparities in the distribution of risk exposure. In this paper, we propose that SES indicators will be expected to spatially cluster vulnerable individuals and groups into heavily polluted areas. To test this hypothesis, we conducted a set of spatial autocorrelations using 2017–2019 data from governmental records. This study demonstrates the presence of socioeconomic disparities in air pollution exposure in Mexico City. Low-socioeconomic-status populations located in the southern periphery were exposed to greater concentrations of O₃. Our spatial analyses for NO₂ and CO shows, however, that greater exposure was observed in the city's center, the wealthiest core of Mexico City. Our results agree with studies performed in other cities worldwide which argued that populations of high socioeconomic status usually positioned themselves in the city center, where there is a high vehicular flow and a great concentration of economic activities. Our findings highlight the need for policy-driven approaches that take into consideration air pollution geographic variability, meteorological variability, and the main drivers of socioeconomic inequality to mitigate air pollution exposure and potential economic and health impacts.

Author Contributions: Conceptualization, Y.M., J.G.-B., E.V., A.R.-O., A.N. and J.M.M.-A.; methodology, J.G.-B., A.R.-O., Y.M., E.V., C.G.R.-M. and M.J.-P.; formal analysis, J.G.-B., A.R.-O. and Y.M.; writing—original draft preparation, Y.M.; writing—review and editing, visualization, L.B., L.H., A.P., J.E., J.C.N.-E. and R.M. All authors have read and agreed to the published version of the manuscript.

Funding: This research was funded by the Secretaria de Educación, Ciencia, Tecnología e Innovación funded project (Award No. SECTEI/203/2019, Mexico) and the British Council (Award No. 527635178).

Informed Consent Statement: Not applicable.

Data Availability Statement: Not applicable.

Acknowledgments: We acknowledge the support of the Secretaría del Medio Ambiente for their participation during the development of this study.

Conflicts of Interest: The authors declare no conflict of interest.

Appendix A

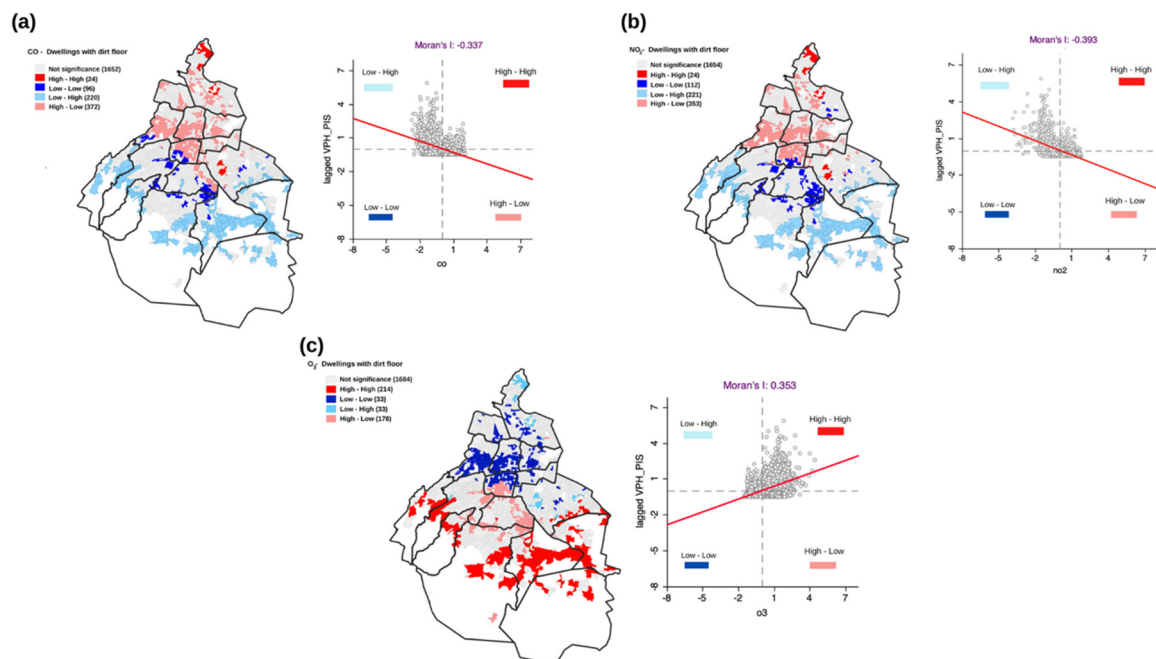


Figure A1. Moran's scatterplots for (a) NO₂, (b) CO and (c) O₃ exposure by number of houses on dirt floors (VPH_PISOTI) in Mexico City. Scatterplots consist of four quadrants: High-High (hotspots-environmental inequalities), Low-High (outliers), Low-Low (coldspots) and High-Low (outliers).

Table A1. 2017–2019 average relative humidity (%), temperature (°C) and wind speed (m/s²) for the dry-cold (November to February), dry-warm (March to May), and wet (June to October) seasons calculated in each of the 26 monitoring stations derived from the Meteorology Network (REDMET).

Station	Dry-Cold			Dry-Warm			Wet		
	RH Mean ± SD	T °C Mean ± SD	WS Mean ± SD	RH Mean ± SD	T °C Mean ± SD	WS Mean ± SD	Rh Mean ± SD	T °C Mean ± SD	WS Mean ± SD
ACO	59.9 ± 22	17.6 ± 4.6	2.4 ± 1.4	47.1 ± 22.7	18.2 ± 5.6	2.6 ± 1.5	67.0 ± 18.1	17.3 ± 3.8	2.3 ± 1.3
AJU	72.1 ± 21.9	11.9 ± 4.2	2.5 ± 1.1	41.1 ± 18.5	17.7 ± 3.9	3.2 ± 1.8	63.6 ± 16.6	16.5 ± 2.9	2.6 ± 1.3
AJM	54.5 ± 20.6	17.0 ± 3.4	2.8 ± 1.5	62.7 ± 24.1	11.7 ± 5.5	2.9 ± 1.3	79.7 ± 16.5	12.0 ± 3.4	2.2 ± 1.0
BJU	54.0 ± 20.8	18.8 ± 3.8	1.8 ± 0.9	42.1 ± 19.6	19.5 ± 4.5	1.9 ± 1.0	61.3 ± 18.0	18.4 ± 3.3	1.8 ± 0.8
CHO	58.7 ± 20.6	17.7 ± 4.3	1.7 ± 1.1	45.6 ± 19.6	18.3 ± 5.2	1.8 ± 1.2	67.6 ± 16.0	17.2 ± 3.6	1.6 ± 1.1
CUA	59.3 ± 21.3	15.2 ± 3.6	2.0 ± 0.9	44.4 ± 19.3	16.3 ± 4.0	2.2 ± 1.0	68.8 ± 16.6	14.6 ± 3.1	1.9 ± 0.9
CUT	65.0 ± 24.2	16.8 ± 5.2	1.6 ± 0.9	52.8 ± 26.8	16.8 ± 7.0	1.7 ± 1.0	71.6 ± 19.8	16.8 ± 4.2	1.6 ± 0.8
FAC	55.6 ± 24.0	18.5 ± 5.7	1.8 ± 0.9	43.0 ± 22.9	19.1 ± 6.8	1.9 ± 1.0	63.5 ± 21.1	18.2 ± 4.9	1.8 ± 0.9
GAM	58.5 ± 21.0	19.2 ± 4.0	2.0 ± 1.3	46.1 ± 20.1	20.0 ± 4.7	2.1 ± 1.3	66.1 ± 17.8	18.8 ± 3.4	2.0 ± 1.2
HGM	51.1 ± 19.4	18.9 ± 3.7	1.9 ± 1.1	37.8 ± 17.9	19.9 ± 4.3	1.9 ± 1.2	57.4 ± 16.8	18.4 ± 3.3	1.9 ± 1.0
INN	69.0 ± 22.5	11.5 ± 5.5	1.6 ± 0.9	57.4 ± 23.3	11.4 ± 5.9	1.8 ± 1.1	79.1 ± 16.2	11.8 ± 3.7	1.4 ± 0.8
LAA	58.5 ± 23.4	18.2 ± 4.3	1.9 ± 0.9	44.2 ± 21.5	19.1 ± 5.1	1.9 ± 1.0	67.0 ± 20.1	17.8 ± 3.7	1.9 ± 0.9
MER	54.8 ± 20.9	18.8 ± 3.8	2.2 ± 1.0	42.1 ± 19.9	19.7 ± 4.5	2.2 ± 1.2	62.4 ± 17.6	18.3 ± 3.3	2.2 ± 1.0
MGH	50.8 ± 21.4	18.8 ± 3.9	2.1 ± 1.0	37.0 ± 19.2	19.8 ± 4.5	2.2 ± 1.1	59.2 ± 18.1	18.2 ± 3.3	2.0 ± 0.9
MON	59.1 ± 22.1	18.3 ± 5.0	2.2 ± 1.5	46.4 ± 21.9	18.9 ± 6.1	2.4 ± 1.6	67.3 ± 18.0	18.0 ± 4.2	2.0 ± 1.5
MPA	59.0 ± 20.1	16.2 ± 3.8	2.8 ± 1.3	44.2 ± 19.2	17.7 ± 4.4	3.3 ± 1.6	67.8 ± 14.8	15.3 ± 3.1	2.5 ± 1.1
NEZ	54.0 ± 19.8	17.8 ± 3.9	2.5 ± 1.3	42.1 ± 19.1	18.7 ± 4.6	2.6 ± 1.5	61.4 ± 16.3	17.2 ± 3.3	2.5 ± 1.3
PED	56.0 ± 21.3	18.1 ± 3.9	1.9 ± 0.9	42.4 ± 19.2	19.1 ± 4.5	2.2 ± 1.1	64.3 ± 17.9	17.6 ± 3.3	1.9 ± 0.8
SAG	48.3 ± 21.7	19.6 ± 4.1	1.6 ± 0.8	37.2 ± 20.1	20.3 ± 4.8	1.5 ± 0.8	56.3 ± 19.2	19.2 ± 3.5	1.6 ± 0.9
SFE	58.7 ± 21.8	16.0 ± 3.6	2.3 ± 1.0	43.8 ± 19.4	17.1 ± 4.3	2.7 ± 1.0	69.1 ± 16.7	15.4 ± 3.0	2.2 ± 0.9
TAH	54.5 ± 20.2	18.0 ± 4.2	2.1 ± 1.1	39.9 ± 19.4	19.0 ± 5.1	2.3 ± 1.4	61.4 ± 16.7	17.6 ± 3.6	2.0 ± 1.0
TLA	52.0 ± 19.9	18.0 ± 4.0	2.1 ± 1.1	39.7 ± 19.1	18.7 ± 4.8	2.1 ± 1.2	59.3 ± 16.5	17.6 ± 3.4	2.2 ± 1.1
UAX	55.6 ± 20.7	18.5 ± 4.1	2.0 ± 1.0	44.6 ± 20.0	19.0 ± 4.8	2.2 ± 1.2	62.9 ± 17.7	18.1 ± 3.5	1.9 ± 0.9
UIZ	56.7 ± 21.5	19.2 ± 3.7	2.2 ± 1.1	44.7 ± 20.7	20.2 ± 4.6	2.3 ± 1.3	64.0 ± 18.5	18.9 ± 3.5	2.2 ± 1.1
VIF	56.9 ± 22.6	18.5 ± 4.5	2.0 ± 1.1	44.7 ± 22.4	19.2 ± 5.4	2.0 ± 1.2	64.2 ± 19.4	18.0 ± 3.7	2.0 ± 1.1
XAL	51.3 ± 18.9	18.2 ± 3.6	2.9 ± 2.0	39.3 ± 18.3	19.0 ± 4.3	2.8 ± 2.1	57.7 ± 15.8	17.9 ± 3.1	2.9 ± 2.0
Average	57.0	17.5	2.1	42.9	18.2	2.3	65.1	17.1	2.1

Table A2. Significant Pearson correlation coefficients ($\alpha = 0.05$) among socioeconomic status indicators. SES indicators with positive coefficients $r \leq 0.6$ were kept for further analyses. The selected SES indicators and associated correlation coefficients are shown in bold. IMU2010: urban marginalization index; POBTOT: total population; POBFEM: female population; POBMAS: male population; P0A20 and P_3A5: children population younger than 5 years old; P_60YMAS: population older than 60 years old; P_HOG_IND: indigenous population; PCON_DISC: population with disabilities; PSINDER: population without access to health care; VPH_PISOTI: number of houses on dirt floors; VPH_S_ELEC: number of hoses without electricity; VPH_AGUAFV: number of houses without access to potable water; VPH_NODRAIN: number of houses without a drainage system; VPH_NDACMM: number of houses lacking access to private motorized transport; VPH_SINTIC: number of houses without access to communication technologies.

	IMU2010	POBTOT	POBFEM	POBMAS	P_0A20	P_3A5	P_60YMAS	PHOG_IND	PCON_DISC	PSINDER	VPH_PISOTI	VPH_S_ELEC	VPH_AGUAFV	VPH_NODRAIN	VPH_NDA_CMM	VPH_SIN_TIC
IMU2010	1	0.3	0.3	0.4	0.5	0.5	0.0	0.6	0.4	0.5	0.6	0.4	0.4	0.4	0.4	0.5
POBTOT	0.3	1	1	1	0.9	0.9	0.8	0.7	0.8	0.9	0.4	0.3	0.2	0.3	0.9	0.5
POBFEM	0.3	1	1	1	0.9	0.9	0.8	0.7	0.8	0.9	0.4	0.3	0.2	0.3	0.9	0.5
POBMAS	0.4	1	1	1	0.9	0.9	0.8	0.7	0.8	0.9	0.4	0.3	0.2	0.3	0.9	0.6
P_0A20	0.5	0.9	0.9	0.9	1	0.9	0.7	0.7	0.8	0.9	0.5	0.4	0.3	0.4	0.8	0.6
P_3A5	0.5	0.9	0.9	0.9	0.9	1	0.7	0.7	0.8	0.9	0.5	0.4	0.3	0.4	0.9	0.6
P_60YMAS	0.0	0.8	0.8	0.8	0.7	0.7	1	0.3	0.7	0.7	0.1	0.1	0.0	0.1	0.7	0.3
PHOG_IND	0.6	0.7	0.7	0.7	0.7	0.7	0.3	1	0.6	0.7	0.6	0.5	0.5	0.6	0.6	0.6
PCON_DISC	0.4	0.8	0.8	0.8	0.8	0.8	0.7	0.6	1	0.8	0.4	0.3	0.2	0.3	0.8	0.5
PSINDER	0.5	0.9	0.9	0.9	0.9	0.9	0.7	0.7	0.8	1	0.5	0.4	0.2	0.3	0.9	0.6
VPH_PISOTI	0.6	0.4	0.4	0.4	0.5	0.5	0.1	0.6	0.4	0.5	1	0.6	0.5	0.6	0.4	0.5
VPH_S_ELEC	0.4	0.3	0.3	0.3	0.4	0.4	0.1	0.5	0.3	0.4	0.6	1	0.4	0.6	0.3	0.5
VPH_AGUAFV	0.4	0.2	0.2	0.2	0.3	0.3	0.0	0.5	0.2	0.2	0.5	0.4	1	0.6	0.2	0.3
VPH_NODRAIN	0.4	0.3	0.3	0.3	0.4	0.4	0.1	0.6	0.3	0.3	0.6	0.6	0.6	1	0.3	0.4
VPH_NDACMM	0.4	0.9	0.9	0.9	0.8	0.9	0.7	0.7	0.8	0.9	0.4	0.3	0.2	0.3	1	0.6
VPH_SINTIC	0.5	0.5	0.5	0.6	0.6	0.6	0.3	0.6	0.5	0.6	0.5	0.5	0.3	0.4	0.6	1

Table A3. Value estimates for the nugget, psill and range parameters obtained in the theoretical semivariograms and the models that best fit the observed data for each pollutant.

Estimate	Pollutant				
	PM _{2.5}	PM ₁₀	O ₃	CO	NO ₂
Nugget	5.3	134.4	0	0	0
Psill	254.6	1297.6	18.5	0.01	30.1
Range	59.9	10.8	21.4	26.4	4.2
Model	Gaussian	Materon	Materon	Lineal	Materon

Appendix B

Table A4. Glossary of SES indicators.

SES Indicator	Description
POBTOT	Total population
POPMAS	Total male population
POP_FEM	Total female population
P_HOG_IND	Population who declared speaking an indigenous language or considered themselves as indigenous
POBAFRO	Population who considers themselves Afro-Mexican or Afro-descendant
PCON_DIS	Population with disabilities that perform with great difficulties
P_60YMAS	Population aging 60 to 130 years
P_0A2 and P_3A5	Population younger than 5 years old.
PSINDER	Population without access to health services
VPH_PISOTI	Number of houses with dirt floors.
VPH_S_ELEC	Number of houses without electricity.
VPH_NODRAIN	Number of houses without drainage connection
VPH_AGUAFV	Number of houses without access to potable water
VPH_NDACMM	Number of houses lacking access to private motorized transport
VPH_SINTIC	Number of houses without technology
IMU2010	Compound index built on different inequality dimensions such as access to education and health care, availability of first-order goods, of and enjoyment of adequate housing rights

Glossary of Equations

1. Spatial Distribution of Air Pollutants

Equation (A1).

$$\sum_{i=1}^n \lambda_i \gamma [d(S_i, S_j)] + m = \gamma [d(S_o, S_i)], \quad i = 1, \dots, n; \quad \sum_{i=1}^n \lambda_i = 1 \quad (\text{A1})$$

where n is the number of observations for each measured variable, m is the Lagrange multiplier used to derive local maxima and minima of a function subjected to equality constraints, λ is the weight given to each of the observations; in our case, we assumed all observations have equal weights and γ is the semivariogram. The sum of all observation weights must be equal to one. In Equation (A1), S is the measured variable at a given sample point (monitoring station); in our case, the calculated annual 2017–2019 average

concentrations for O₃, NO₂ and CO, and the 90th percentile of daily average concentrations for PM₁₀ and PM_{2.5}; the subscript 0 is the estimation point (unknown) and the subscripts *i* and *j* corresponded to the coordinates of the observed sample point. Finally, the term $d(S_i, S_0)$ represented the distance between observed and unknown points estimated from the semivariogram using Equation (A2):

Equation (A2).

$$\gamma[d(S_i, S_0)] = \text{var}[z(S_i) - z(S_0)] \quad (\text{A2})$$

2. Spatial Autocorrelation Index

Equation (A3).

$$I_{X,Y} = \frac{\sum_i \sum_j \omega_{ij} (x_i - \bar{x})(y_i - \bar{y})}{\sqrt{\sum (x_i - \bar{x})^2} \sqrt{\sum (y_j - \bar{y})^2}} \quad (\text{A3})$$

where W_{ij} are the elements of the contiguity matrix (Queen); $(x_i - \text{mean}(x_i))$ and $(y_i - \text{mean}(y_i))$ are normalized values of variables *X* and *Y* in location *i* and *j*.

References

- IPCC Summary for Policymakers. *Climate Change 2022: Impacts, Adaptation and Vulnerability. Contribution of Working Group II to the Sixth Assessment Report of the Intergovernmental Panel on Climate*; Pörtner, H.-O., Roberts, D.C., Poloczanska, E.S., Mintenbeck, K., Tignor, M., Alegria, A., Craig, M., Langsdorf, S., Löschke, S., Möller, V., et al., Eds.; Cambridge University Press: Cambridge, UK; New York, NY, USA, 2022; pp. 3–33. [CrossRef]
- Xiao, X.; Gao, M. Overview of climate change, air pollution, and human health. In *Air Pollution, Climate, and Health: An Integrated Perspective on Their Interactions*; Gao, M., Wang, Z.F., Carmichael, G., Eds.; Elsevier: Amsterdam, The Netherlands, 2021; Volume 12, pp. 3–12. [CrossRef]
- Kelly, F.J.; Fussell, J.C. Air Pollution and Public Health: Emerging Hazards and Improved Understanding of Risk. *Environ. Geochem. Health* **2015**, *37*, 631–649. [CrossRef] [PubMed]
- World Health Organization (WHO). Environmental Health Inequalities in Europe: Assessment Report. 2012. Available online: <https://apps.who.int/iris/bitstream/handle/10665/107299/e96194.pdf?sequence=1> (accessed on 12 July 2022).
- Environmental Protection Agency (EPA). Air Quality Criteria for Particulate Matter (Final Report, 1996). Risk Assessment Portal. US EPA. 1996. Available online: <https://cfpub.epa.gov/ncea/risk/recordisplay.cfm?deid=2832> (accessed on 12 July 2022).
- Islam, S.N.; Winkel, J. Climate Change and Social Inequality. DESA Working Paper 152. Department of Economic & Social Affairs, United Nations. 2017. Available online: <https://www.un.org/development/desa/publications/working-paper/wp152> (accessed on 12 July 2022).
- Wenz, P.S. *Environmental Justice*; State University of New York Press: Albany, NY, USA, 1988; Available online: <https://sunypress.edu/Books/E/Environmental-Justice> (accessed on 12 July 2022).
- Chakraborty, J.; Basu, P. Linking Industrial Hazards and Social Inequalities: Environmental Injustice in Gujarat, India. *Int. J. Environ. Res. Public Health* **2018**, *16*, 42. [CrossRef] [PubMed]
- Ferguson, L.; Taylor, J.; Davies, M.; Shrubsole, C.; Symonds, P.; Dimitroulopoulou, S. Exposure to Indoor Air Pollution across Socio-Economic Groups in High-Income Countries: A Scoping Review of the Literature and a Modelling Methodology. *Environ. Int.* **2020**, *143*, 105748. [CrossRef] [PubMed]
- Hajat, A.; Hsia, C.; O'Neill, M.S. Socioeconomic Disparities and Air Pollution Exposure: A Global Review. *Curr. Environ. Health Rep.* **2015**, *2*, 440–450. [CrossRef] [PubMed]
- Harper, S.; Ruder, E.; Roman, H.; Geggel, A.; Nweke, O.; Payne-Sturges, D.; Levy, J. Using Inequality Measures to Incorporate Environmental Justice into Regulatory Analyses. *Int. J. Environ. Res. Public Health* **2013**, *10*, 4039–4059. [CrossRef]
- Chakraborti, L.; Shimshack, J.P. Environmental Disparities in Urban Mexico: Evidence from Toxic Water Pollution. *Resour. Energy Econ.* **2022**, *67*, 101281. [CrossRef]
- Eakin, H.; Parajuli, J.; Yogya, Y.; Hernández, B.; Manheim, M. Entry Points for Addressing Justice and Politics in Urban Flood Adaptation Decision Making. *Curr. Opin. Environ. Sustain.* **2021**, *51*, 1–6. [CrossRef]
- Reed, P.M.; Hadjimichael, A.; Moss, R.H.; Brelford, C.; Burleyson, C.D.; Cohen, S.; Dyreson, A.; Gold, D.F.; Gupta, R.S.; Keller, K.; et al. Multisector Dynamics: Advancing the Science of Complex Adaptive Human-Earth Systems. *Earths Future* **2022**, *10*, 1–18. [CrossRef]
- Eakin, H.; Bojórquez-Tapia, L.A.; Janssen, M.; Georgescu, M.; Manuel-Navarrete, D.; Vivoni, E.R.; Escalante, A.E.; Baeza-Castro, A.; Mazari-Hiriart, M.; Lerner, A.M. Urban resilience efforts must consider social and political forces. *Proc. Natl. Acad. Sci. USA* **2017**, *114*, 186–189. [CrossRef]
- Li, M.; Du, W. Can internet development improve energy efficiency of firms: Empirical evidence from China. *Energy* **2021**, *237*, 121590. [CrossRef]
- Doss-Gollin, J.; Farnham, D.J.; Steinschneider, S.; Lall, U. Robust Adaptation to Multiscale Climate Variability. *Earths Future* **2019**, *7*, 734–747. [CrossRef]

18. Namdeo, A.; Stringer, C. Investigating the relationship between air pollution, health and social deprivation in Leeds, UK. *Environ. Int.* **2008**, *34*, 585–591. [[CrossRef](#)] [[PubMed](#)]
19. Flanagan, E.; Mattisson, K.; Waller, J.; Abera, A.; Eriksson, A.; Balidemaj, F.; Oudin, A.; Isaxon, C.; Malmqvist, E. Air Pollution and Urban Green Space: Evidence of Environmental Injustice in Adama, Ethiopia. *Front. Sustain. Cities* **2021**, *3*, 728384. [[CrossRef](#)]
20. Marshall, J.D. Environmental Inequality: Air Pollution Exposures in California's South Coast Air Basin. *Atmos. Environ.* **2008**, *42*, 5499–5503. [[CrossRef](#)]
21. Morello-Frosch, R.; Pastor, M.; Porras, C.; Sadd, J. Environmental Justice and Regional Inequality in Southern California: Implications for Future Research. *Environ. Health Perspect.* **2002**, *110*, 149–154. [[CrossRef](#)]
22. Barnes, J.H.; Chatterton, T.J.; Longhurst, J.W.S. Emissions vs Exposure: Increasing Injustice from Road Traffic-Related Air Pollution in the United Kingdom. *Transp. Res. Part D Transp. Environ.* **2019**, *73*, 56–66. [[CrossRef](#)]
23. Samoli, E.; Stergiopoulou, A.; Santana, P.; Rodopoulou, S.; Mitsakou, C.; Dimitroulopoulou, C.; Bauwelinck, M.; de Hoogh, K.; Costa, C.; Mari-Dell'Olmo, M.; et al. Spatial Variability in Air Pollution Exposure in Relation to Socioeconomic Indicators in Nine European Metropolitan Areas: A Study on Environmental Inequality. *Environ. Pollut.* **2019**, *249*, 345–353. [[CrossRef](#)]
24. Lomé-Hurtado, A.; Touza-Montero, J.; White, P.C.L. Environmental Injustice in Mexico City: A Spatial Quantile Approach. *Exp. Health* **2020**, *12*, 265–279. [[CrossRef](#)]
25. Instituto Nacional de Estadística, Geografía e Informática (INEGI). Censo de Población y Vivienda. 2020. Available online: <https://www.inegi.org.mx/programas/ccpv/2020/> (accessed on 13 July 2022).
26. López Vázquez, V.H.; Plata Rocha, W. Análisis de Los Cambios de Cobertura de Suelo Derivados de La Expansión Urbana de La Zona Metropolitana de La Ciudad de México, 1990–2000. *Investig. Geográficas* **2009**, *68*, 85–101.
27. Romero Lankao, P. Water in Mexico City: What Will Climate Change Bring to Its History of Water-Related Hazards and Vulnerabilities? *Environ. Urban.* **2010**, *22*, 157–178. [[CrossRef](#)]
28. Secretaría del Medio Ambiente de la Ciudad de México (SEDEMA). Informe de Calidad Del Aire En La Ciudad de México. 2016. Available online: <http://www.aire.cdmx.gob.mx/descargas/publicaciones/flippingbook/informe-2016-calidad-del-aire-en-la-ciudad-de-mexico/mobile/index.html> (accessed on 12 July 2022).
29. Instituto Nacional de Estadística, Geografía e Informática-Directorio Estadístico Nacional de Unidades Económicas (INEGI-DNUE). Directorio de Empresas y Establecimientos. 2022. Available online: <https://www.inegi.org.mx/temas/directorio/> (accessed on 12 July 2022).
30. Bell, M.L.; Davis, D.L.; Gouveia, N.; Borja-Aburto, V.H.; Cifuentes, L.A. The Avoidable Health Effects of Air Pollution in Three Latin American Cities: Santiago, São Paulo, and Mexico City. *Environ. Res.* **2006**, *100*, 431–440. [[CrossRef](#)] [[PubMed](#)]
31. Vega, E.; Namdeo, A.; Bramwell, L.; Miquelajauregui, Y.; Resendiz-Martinez, C.G.; Jaimes-Palomera, M.; Luna-Falfan, F.; Terrazas-Ahumada, A.; Maji, K.J.; Entwistle, J.; et al. Changes in Air Quality in Mexico City, London and Delhi in Response to Various Stages and Levels of Lockdowns and Easing of Restrictions during COVID-19 Pandemic. *Environ. Pollut.* **2021**, *285*, 117664. [[CrossRef](#)] [[PubMed](#)]
32. Mamkhezri, J.; Bohara, A.K.; Islas Camargo, A. Air Pollution and Daily Mortality in the Mexico City Metropolitan Area. *Atmósfera* **2020**, *33*, 249–267. [[CrossRef](#)]
33. Consejo Nacional de Población (CONAPO). Índices de Marginación 2010. Consejo Nacional de Población. 2010. Available online: <https://www.gob.mx/conapo/documentos/indices-de-marginacion-2020-284372> (accessed on 13 July 2022).
34. Wu, Y.-H.; Hung, M.-C. Comparison of Spatial Interpolation Techniques Using Visualization and Quantitative Assessment. In *Applications of Spatial Statistics*; IntechOpen: Oxford, UK, 2016.
35. Armstrong, M. *Basic Linear Geostatistics*; Springer: Berlin, Germany, 1998.
36. Deligiorgi, D.; Philippopoulos, K. Spatial interpolation methodologies in urban air pollution modeling: Application for the greater area of metropolitan Athens, Greece. *Adv. Air Pollut.* **2011**, *17*, 10.
37. Willmott, C.J. Some Comments on the Evaluation of Model Performance. *Bull. Am. Meteorol. Soc.* **1982**, *63*, 1309–1313. [[CrossRef](#)]
38. Getis, A. A History of the Concept of Spatial Autocorrelation: A Geographer's Perspective. *Geogr. Anal.* **2008**, *40*, 297–309. [[CrossRef](#)]
39. Wartenberg, D. Multivariate Spatial Correlation: A Method for Exploratory Geographical Analysis. *Geogr. Anal.* **2010**, *17*, 263–283. [[CrossRef](#)]
40. Negreiros, R.L.; Amaku, M.; Dias, R.A.; Ferreira, F.; Cavalléro, J.C.M.; Ferreira Neto, J.S. Spatial Clustering Analysis of the Foot-and-Mouth Disease Outbreaks in Mato Grosso Do Sul State, Brazil—2005. *Ciência Rural*. **2009**, *39*, 2609–2613. [[CrossRef](#)]
41. Anselin, L. Local Indicators of Spatial Association-LISA. *Geogr. Anal.* **2010**, *27*, 93–115. [[CrossRef](#)]
42. Han, S.; Bian, H.; Feng, Y.; Liu, A.; Li, X.; Zeng, F.; Zhang, X. Analysis of the Relationship between O₃, NO and NO₂ in Tianjin, China. *Aerosol Air Qual. Res.* **2011**, *11*, 128–139. [[CrossRef](#)]
43. Anselin, L.; Syabri, I.; Kho, Y. GeoDa: An Introduction to Spatial Data Analysis. In *Handbook of Applied Spatial Analysis*; Springer: Berlin/Heidelberg, Germany, 2010; pp. 73–89. [[CrossRef](#)]
44. R Core Team. *R: A Language and Environment for Statistical Computing*; R Foundation for Statistical Computing: Vienna, Austria, 2021; Available online: <https://www.R-project.org/> (accessed on 14 March 2022).
45. Salonen, H.; Salthammer, T.; Morawska, L. Human Exposure to Ozone in School and Office Indoor Environments. *Environ. Int.* **2018**, *119*, 503–514. [[CrossRef](#)] [[PubMed](#)]

46. Tellman, B.; Eakin, H.; Janssen, M.A.; de Alba, F.; Turner II, B.L. The Role of Institutional Entrepreneurs and Informal Land Transactions in Mexico City's Urban Expansion. *World Dev.* **2021**, *140*, 105374. [[CrossRef](#)]
47. Gilbert, L.; de Jong, F. Entanglements of Periphery and Informality in Mexico City. *Int. J. Urban Reg. Res.* **2015**, *39*, 518–532. [[CrossRef](#)]
48. Aguilar, A.G.; Flores, M.A.; Lara, L.F. Peri-urbanization and land use fragmentation in Mexico City. Informatlity, environmental deterioration and ineffective urban policy. *Front. Sustain. Cities* **2022**, *4*, 1–19. [[CrossRef](#)]
49. Baeza, A.; Estrada-Barón, A.; Serrano-Candela, F.; Bojórquez, L.A.; Eakin, H.; Escalante, A.E. Biophysical, Infrastructural and Social Heterogeneities Explain Spatial Distribution of Waterborne Gastrointestinal Disease Burden in Mexico City. *Environ. Res. Lett.* **2018**, *13*, 064016. [[CrossRef](#)]
50. Potoczek, A.; Bukowski, M.; Jasko, K.; Czepluch, F.; Fritsche, I.; Jugert, P.; Kossowska, M. Acting Collectively against Air Pollution: When Does Control Threat Mobilize Environmental Activism? *Registered Report. J. Exp. Soc. Psychol.* **2022**, *102*, 104352. [[CrossRef](#)]
51. Consejo de Evaluación del Desarrollo Social de la Ciudad de México. Ciudad de México 2020: Un Diagnóstico de la Desigualdad Socio Territorial. 2020. Available online: <https://www.evalua.cdmx.gob.mx/estudios-e-investigaciones/ciudad-de-mexico-2020-un-diagnostico-de-la-desigualdad-socio-territorial> (accessed on 13 July 2022).
52. Guerra, E.; Caudillo, C.; Monkkonen, P.; Montejano, J. Urban Form, Transit Supply, and Travel Behavior in Latin America: Evidence from Mexico's 100 Largest Urban Areas. *Transp. Policy* **2018**, *69*, 98–105. [[CrossRef](#)]
53. Cooper, N.; Green, D.; Knibbs, L.D. Inequalities in Exposure to the Air Pollutants PM_{2.5} and NO₂ in Australia. *Environ. Res. Lett.* **2019**, *14*, 115005. [[CrossRef](#)]
54. Chakraborty, J. Children's Exposure to Vehicular Pollution: Environmental Injustice in Texas, USA. *Environ. Res.* **2022**, *204*, 112008. [[CrossRef](#)]
55. Cortese, A.D.; Spengler, J.D. Ability of Fixed Monitoring Stations to Represent Personal Carbon Monoxide Exposure. *J. Air. Pollut. Control Assoc.* **1976**, *26*, 1144–1150. [[CrossRef](#)]
56. Mohai, P.; Pellow, D.; Roberts, J.T. Environmental Justice. *Annu. Rev. Environ. Resour.* **2009**, *34*, 405–430. [[CrossRef](#)]
57. Miquelajauregui, Y.; Bojórquez-Tapia, L.A.; Eakin, H.; Gómez-Priego, P.; Pedroza-Páez, D. Challenges and opportunities for universities in building adaptive capacities for sustainability: Lessons from Mexico, Central America and the Caribbean. *Clim. Policy* **2022**, *22*, 637–651. [[CrossRef](#)]